Monte-Carlo modelling of multi-conjugate adaptive optics performance on the European Extremely Large Telescope

A. G. Basden[1]⋆
[1]*Department of Physics, South Road, Durham, DH1 3LE, UK*

13 August 2015

ABSTRACT

The performance of a wide-field adaptive optics system depends on input design parameters. Here we investigate the performance of a multi-conjugate adaptive optics system design for the European Extremely Large Telescope, using an end-to-end Monte-Carlo adaptive optics simulation tool, DASP. We consider parameters such as the number of laser guide stars, sodium layer depth, wavefront sensor pixel scale, number of deformable mirrors, mirror conjugation and actuator pitch. We provide potential areas where costs savings can be made, and investigate trade-offs between performance and cost. We conclude that a 6 laser guide star system using 3 DMs seems to be a sweet spot for performance and cost compromise.

Key words: Instrumentation: adaptive optics, Methods: numerical

1 INTRODUCTION

The forthcoming Extremely Large Telescopes (ELTs) (Spyromilio et al. 2008; Nelson & Sanders 2008; Johns 2008) all rely on adaptive optics (AO) systems (Babcock 1953) to provide atmospheric turbulence compensation allowing scientific goals requiring high resolution imaging and spectroscopy to be met. The design of these AO systems requires extensive modelling and simulation to enable performance estimates to be made, and to explore relevant parameter spaces. Current modelling tools fall into two broad categories: analytical models, and Monte-Carlo simulations. Monte-Carlo simulations, while generally computationally expensive for ELT-scale models, have the ability to deliver high fidelity performance estimates, and include non-linear effects, and as much system detail as is necessary (at the expense of computational requirements).

Here, we use the Durham AO simulation platform (DASP) (Basden et al. 2007; Basden & Myers 2012) to model expected AO performance for a multi-conjugate adaptive optics (MCAO) instrument on the 39 m European ELT (E-ELT). DASP is a Monte-Carlo end-to-end simulation tool, that includes models of the atmosphere, telescope, wavefront sensors, deformable mirrors, AO real-time control system, and performance characterisation via generation of science point spread function (PSF) images. We investigate AO performance as a function of the number of laser guide stars (LGSs) (Foy & Labeyrie 1985), the number of deformable mirrors (DMs), DM actuator pitch and conjugate height, and explore performance across the tele-

scope field of view. We also investigate the degree of elongation of LGSs, which is determined by sodium layer depth in the mesosphere, and the impact of wavefront sensor (WFS) pixel scale on AO performance under different signal-to-noise regimes. Our findings can be used to aid instrument design decisions and to estimate expected AO performance for future instruments, and are complementary to results from other modelling tools for ELT MCAO instrumentation, for example Arcidiacono et al. (2014); Le Louarn et al. (2012).

In §2 we describe our input models and the explored parameter space and in §3 we present the performance estimates obtained. We conclude in §4.

2 MODELLING OF AN E-ELT MCAO SYSTEM

We use DASP to investigate different configurations for a MCAO system on the E-ELT. In the study presented here, we usually consider only the use of LGSs, in order to simplify our results. We assume that the tip-tilt signal from the LGSs is valid, so that natural guide star (NGS) measurements are not necessary. However, we also present results when using low order NGSs for tip-tilt correction (and ignore tip-tilt signal from the LGS when doing so). A previous study has investigated many different NGS asterisms for a multi-object AO (MOAO) instrument on the E-ELT (Basden et al. 2014), and so we do not seek to perform such a study here. We note that the assumption of a valid LGS tip-tilt signal can be both pessimistic and optimistic, depending on NGS asterism, and LGS asterism diameter, since the LGS locations are typically close to the edge of the field of view, while the NGS locations can be spread over the field.

⋆ E-mail: a.g.basden@durham.ac.uk (AGB)

Our key AO performance metric is H-band Strehl ratio (1650 nm), as this is an easily understandable measurement and of particular relevance for imaging cameras, which are typically used behind MCAO systems.

The E-ELT design includes a DM that is part of the telescope structure (the fourth mirror in the optical train). We therefore use this as the ground layer conjugated DM in our modelling, though it is likely that this DM will actually be conjugated a few hundred meters away from ground level, an effect that we investigate.

2.1 Simulation model details

The E-ELT design has four sodium laser launch locations, equally spaced around the telescope just beyond the edge of the telescope aperture, i.e. the lasers are side-launched, rather than centre launched, so that fratricide effects are irrelevant (Otarola et al. 2013). At each launch location, up to two lasers can be launched, with independent pointing possible. In the model that we use here, the launch locations are placed 22 m from the centre of the telescope aperture.

We model the atmosphere using a standard European Southern Observatory (ESO) 35 layer turbulence profile (Sarazin et al. 2013) with an outer scale of 25 m and a Fried's parameter of 13.5 cm at zenith. Investigations into AO performance with variations of this atmospheric profile have been studied previously (Basden et al. 2014), so we do not consider this further here: it is important to realise that the performances derived here are relevant for one atmospheric model only, and that the AO performance will differ under other atmospheric conditions. Our simulations are performed at $30°$ from zenith.

We assume 74×74 sub-apertures for each LGS, and a telescope diameter of 38.55 m, with a central obscuration diameter of 11 m. We model a direction dependant telescope pupil function, since for the E-ELT, the observed central obscuration changes across the field of view. Our model includes the hexagonal pattern of the segmented mirrors, and telescope support structures (spiders), with a representative pupil function shown in Fig. 1.

Our LGS asterism is arranged regularly on a circle, the diameter of which we investigate. The LGS spots are elongated to model a sodium layer at 90 km with a full-width at half-maximum (FWHM) between 5–20 km, and we include the cone effect (or focal anisoplanatism, due to the finite distance) in our simulations. The LGS PSFs are atmospherically broadened to 1 arcsecond, such that the minimum spot size has a 1 arcsecond FWHM along the LGS axis. The LGS photon return is generally assumed to be in the high-light regime (we use 10^6 detected photons per sub-aperture per frame) unless otherwise stated. However, we also investigate more realistic photon flux: the flux from the ESO Wendelstein LGS unit returns between 5–21 million photons per second per m^2 (Bonaccini Calia 2015), depending on location on the sky. With a 500 Hz frame rate and 0.5 m sub-apertures, we can therefore expect between 2500–10000 photons per sub-aperture per frame, with additional reductions due to throughput losses and detector quantum efficiency. We include photon shot noise in our simulations.

We model detector readout noise at 0, 0.1 and 1 electrons rms per pixel, corresponding to typical levels from a noiseless detector (the default case), an electron multiplying
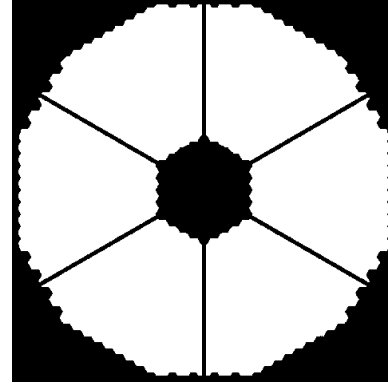

Figure 1. A representitive E-ELT pupil function, for a line of sight 1.5 arcminutes off-axis. The hexagonal pattern of the segmented primary mirror is evident, and a slight vignetting by M4 is seen around the central obscuration (with the effect becoming more pronounced further off-axis). A slight defocusing can also be seen, due to the different conjugate heights of different mirrors in the optical train.

CCD (EMCCD), and a scientific CMOS (sCMOS) detector respectively. For simplicity, we assume that all pixels have the same rms readout noise. This is not the case for sCMOS technology meaning that our results will be slightly optimistic. However, this assumption has been explored elsewhere (Basden 2015).

We include a wavefront slope linearisation algorithm using a look-up table to reduce the effect of non-linearity in the WFS measurements. The LGS wavelength is 589 nm. We measure science PSF performance at 1.65 μm.

We perform tomographic wavefront reconstruction at the conjugate heights of the MCAO DMs using a minimum mean square error (MMSE) algorithm (Ellerbroek et al. 2003) with a Laplacian regularisation to approximate wavefront phase covariance. We assume a WFS frame rate of 500 Hz, and ensure that the science PSFs are well averaged.

The DMs are modelled using a cubic spline interpolation function, which uses given actuator heights and positions to compute a surface map of the DM. The ground layer conjugate DM (M4) has 75×75 actuators, while the pitch of the higher layer conjugate DMs is explored (with the number of required actuators depending on conjugate height, pitch and field of view). We do not consider DM imperfections, as this has been studied previously (Basden 2014).

Unless otherwise stated, we use the following default parameters in the results presented here: 6 LGSs evenly spaced around a 2 arcminute diameter circle, at 90 km with a sodium layer FWHM of 5 km, 3 DMs conjugated to 0 km, 4 km and 12.7 km, with a 1 m actuator pitch (when propagated to the telescope pupil) for the higher DMs, and a 0.52 m actuator pitch for the ground layer DM (equal to the sub-aperture pitch). We note that the assumption of a 5 km FWHM sodium layer is optimistic, however this was chosen to alleviate spot truncation (which is an issue studied elsewhere, e.g. van Dam et al. 2011) when using our default LGS pixel scale of 0.23 arcsec/pixel (chosen to reduce the computational complexity of our simulations). A 10 km
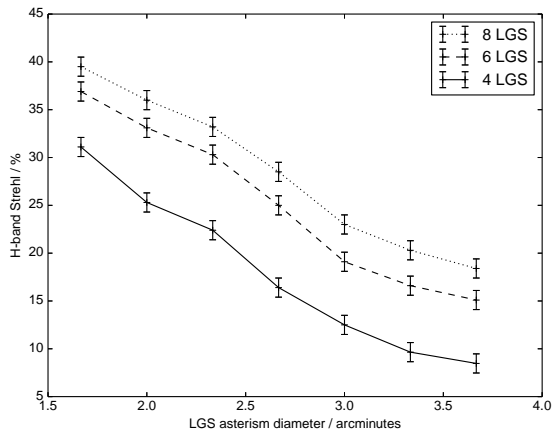
Figure 2. A figure showing on-axis MCAO performance as a function of LGS asterism diameter. The different curves are for different numbers of LGS, as given in the legend.

Figure 4. A figure showing on-axis Strehl ratio as a function of upper DM conjugate height for a 2 DM MCAO system, with 6 LGSs.

width is more typical, while a 20 km width is considered pessimistic. We also note that the DM conjugate heights are chosen to match tentative designs for the first E-ELT MCAO system, and also note that they are similar to the GeMS system on the Gemini South telescope (Rigaut et al. 2012). We use 16×16 pixels per sub-aperture. Results are presented on-axis, except where stated otherwise.

Typically, we run our simulations for 5000 Monte-Carlo iterations, representing 10 s of telescope time, which is sufficient to obtain a well averaged PSF. The uncertainties in our results due to Monte-Carlo randomness are at the 1% level, which we have verified using a suite of separate Monte-Carlo runs.

Figure 5. The C_n^2 profile used in these simulations.

3 PREDICTED PERFORMANCE AND UNCERTAINTIES FOR E-ELT MCAO

A key cost driver for AO instruments on the E-ELT is the number of LGSs required. Fig. 2 shows predicted AO performance at the centre of the field of view as a function of LGS asterism diameter, using different numbers of LGS. It can be seen that, as expected, performance increases with the number of guide stars. However, the gain in performance moving from 6 to 8 LGS (typically 10–20%) is not as significant as moving from 4 to 6 (a 30–70% gain), suggesting that using 6 LGS would present a good trade-off between cost and performance.

Field uniformity is not greatly affected by the number of LGS, as shown in Fig. 3: the predicted AO performance remains reasonably constant across the central 2 arcminutes, independent of the number of LGS used (though with a uniformly lower performance when fewer LGS are used). For comparison, we note that we obtain a H-band Strehl ratio of about 50% when modelling a single conjugate AO (SCAO) system under identical conditions, with 74×74 sub-apertures, high light level assumed, and an integrator control law, in agreement with other studies (Clénet et al. 2011).
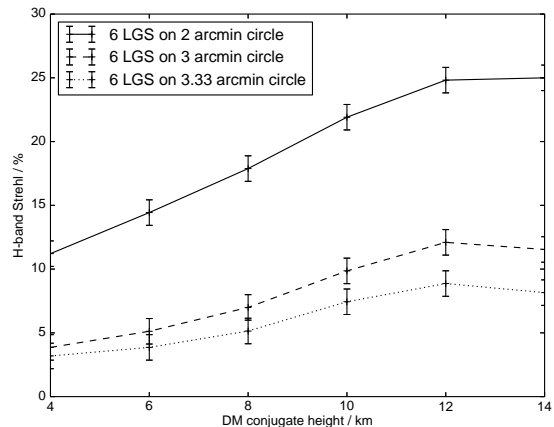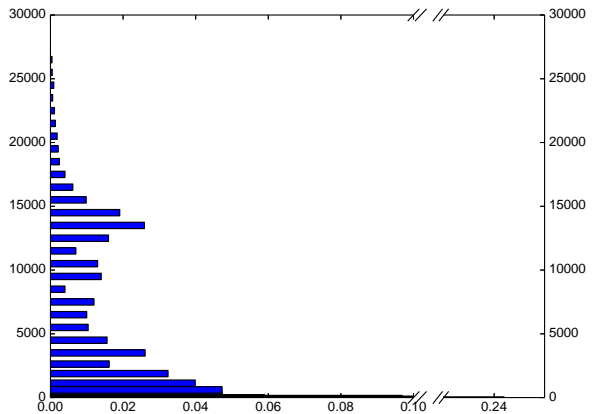
3.1 Dependence on DM conjugation

Fig. 4 shows MCAO performance as a function of DM conjugation height, in the case of a 2 DM system with 6 LGSs, with the lower DM conjugated to ground level. For comparison, the performance with 3 DMs conjugated at 0 km, 4 km and 12.7 km can be taken from Fig. 2. We can see that best performance (for the particular C_n^2 profile used, shown in Fig. 5) is obtained with the upper DM conjugated at 12 km, and that performance with 3 DMs is significantly better than with 2. When compared with the C_n^2 profile (Fig. 4), it is evident that it is important to place the DMs according to where significant turbulence strength lies.

3.2 Dependence on DM actuator pitch

Fig. 6 shows MCAO performance as a function of above-ground DM actuator pitch, for both the 2 DM case (with the upper DM conjugated at 12 km), and the 3 DM case. The pitch of the ground layer DM is maintained at 52 cm. It is evident that using a 1 m actuator pitch for above-ground
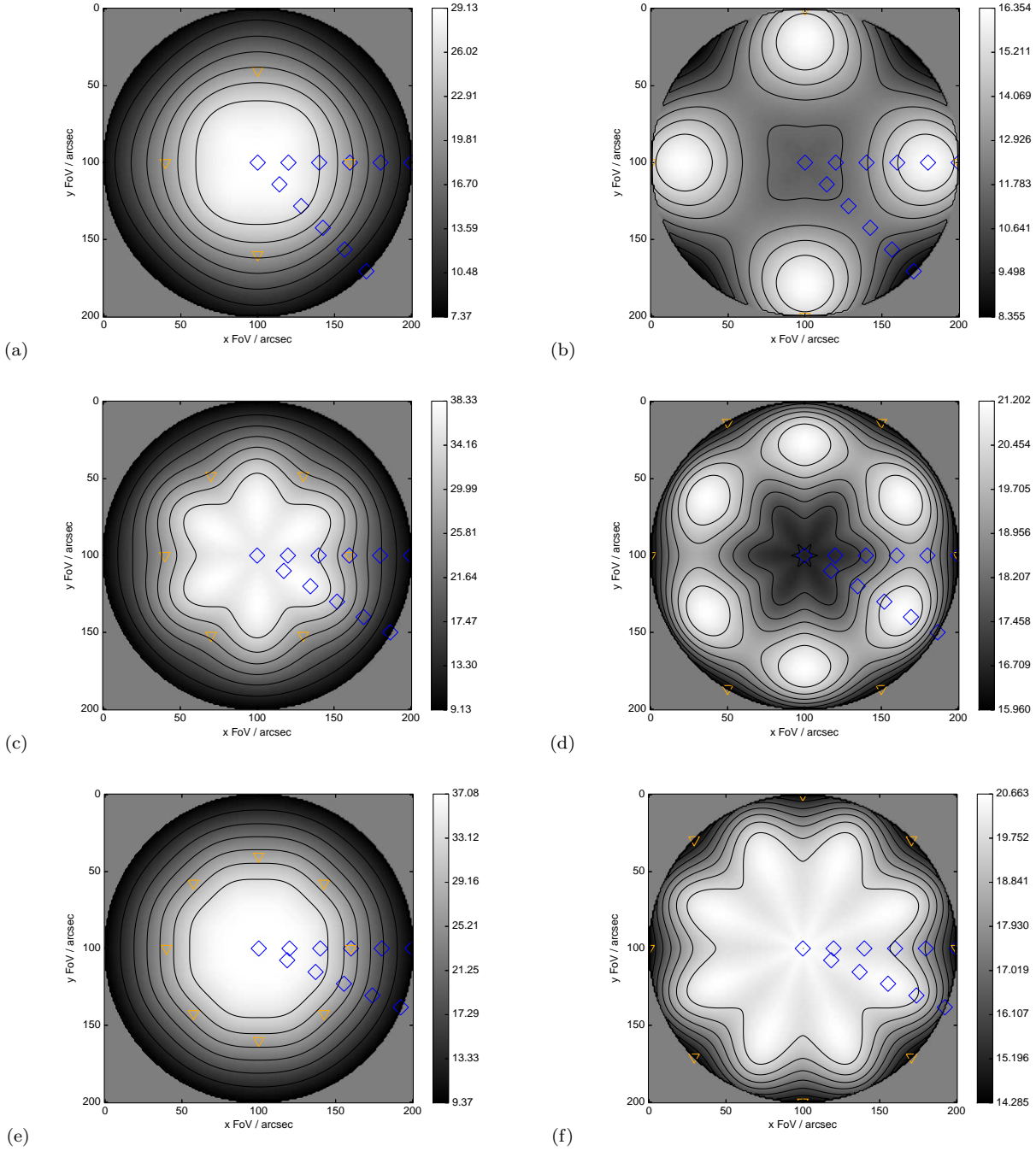
Figure 3. A figure showing MCAO Strehl ratio across a 3.33 arcminute field of view, for: (top row) 4 LGS, (middle row) 6 LGS, (bottom row) 8 LGS, and for (left column) LGS on 2 arcminute diameter ring, (right column) LGS on 3.33 arcminute diameter ring. The LGS positions are shown by orange triangles, and the science PSF sampling locations by blue diamonds.

layer DMs will lead to a small performance degradation, compared to a smaller DM pitch. Using a larger DM actuator pitch results in predicted AO performance falling quickly. A 0.75 m pitch delivers almost identical performance as a 0.5 m pitch. Therefore, when performing a cost benefit analysis, it would seem that the reduction in performance when using a 1 m actuator pitch is acceptable given the cost reduction, but that further increases in pitch would yield significant performance reduction.

3.3   Conjugation height of ground layer DM

The adaptive M4 mirror for the E-ELT is not optically conjugated at ground layer, but rather, a few hundred metres above ground. Fig. 7 shows on-axis AO system performance as a function of ground-layer DM conjugate height, and it is evident that although there may be some variation in performance, this is small over the range of likely conjugate heights, and so can be ignored. We do not take into account the differential conjugate height across the DM that results
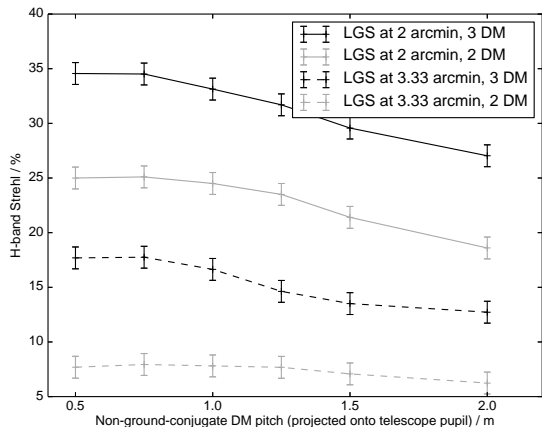
Figure 6. A figure showing on-axis Strehl ratio as a function of above-ground layer DM actuator pitch, for 2 and 3 DMs, and for LGS asterism diameters of 2 and 3.33 arcminutes, as given in the legend.
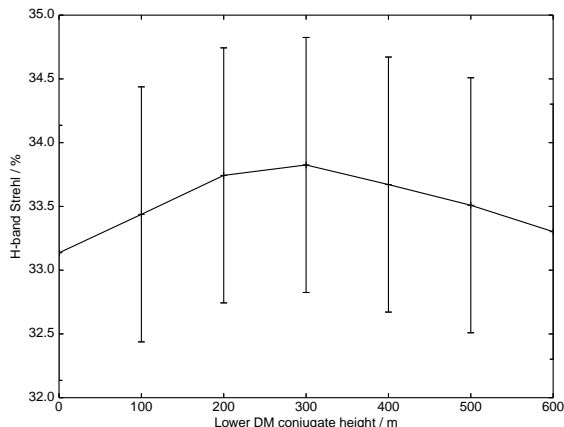

Figure 7. A figure showing on-axis AO performance as a function of lowest DM conjugation height, for a 6 LGS (2 arcminute diameter spacing), 3 DM MCAO system.

from the E-ELT design (i.e. since the DM is tilted, one side has a lower optical conjugate than the other). Instead, we cover the range of conjugate heights.

3.4 Performance variation with LGS pixel scale

The default LGS pixel scale used throughout these simulations equates to 0.23 arcsec/pixel, i.e. a WFS field of view of 3.73 arcsec. This relatively small field of view is used to reduce computational requirements. As a result, our default sodium layer depth is also relatively narrow, at 5 km FWHM to avoid significant spot truncation. Therefore, we investigate AO performance as a function of both pixel scale, and sodium layer depth, as shown in Fig. 8. Since AO performance is highly dependent on sub-aperture noise, which is effected by signal level, detector characteristics, pixel scale and sodium layer depth, we also investigate different noise levels here. It can be seen that in all cases, there is an opti-

mum pixel scale for a given sodium FWHM, signal level and readout noise level. We investigate detected photon fluxes of 100, 1000, 2500, 10000 and 10^6 photons per sub-aperture per frame, and consider readout noise levels of 0, 0.1 and 1 photo-electrons rms (respresenting noiseless, EMCCD and sCMOS technologies). We note that a likely signal level is between 1000–10000 photons per sub-aperture per frame, once throughput losses have been taken into account.

It can be seen that for the lowest signal levels with highest readout noise and largest LGS spots (as seen on the detector, i.e. large sodium layer depth and small pixel scale), that AO correction is very poor, or fails. In these cases, it would probably be possible to fine tune the wavefront reconstruction algorithms, and use an optimal sub-aperture processing algorithm to improve performance. However, we do not consider this here, as such optimisation is beyond the scope of this paper.

At the likely signal levels of between 1000–10000 photons per sub-aperture per frame, and a realistic sodium layer depth FWHM of 10 km, these results suggest that a pixel scale of 0.6–0.7 arcseconds per pixel is reasonable, being robust to changes in the sodium depth (i.e. if the sodium layer depth changes, performance won't be significantly affected). If the sodium layer has a greater extent, then a slightly larger pixel scale (say 0.8 arcseconds per pixel) may be favourable for low signal-to-noise cases.

High signal-to-noise cases (high light level, low readout noise) are seen to favour smaller pixel scales (around 0.4 arcseconds per pixel), due to the increased WFS sensitivity to spot motion (detectable phase gradient resolution). It can also be seen that at these light levels, given the pixel scale is large enough, increasing the sodium layer depth does not significantly impact AO performance, i.e. the performance curve has a broad peak. However, at very low pixel scales, significant truncation of LGS spot images occurs, resulting in reduced performance. With large sodium layer depths, a larger field of view can lead to increased performance, due to reduced spot truncation, and hence higher sensitivity.

We note for the default case (5 km depth, high light level, no noise), that the variation in performance with pixel scale is small (about 10% in Strehl). Therefore, the results presented in the rest of this paper using the default parameters are unlikely to be much different when larger pixel scales are used.

Fig. 9 shows the degree of LGS elongation and truncation for different pixel scales and sodium layer depths for sub-apertures far from the laser launch locations (40 m away). When computing wavefront slopes for these sub-apertures, a conventional centre of gravity algorithm has been used here, and we do not explicitly take into account different slope noise characteristics parallel and perpendicular to the elongation direction, nor do we explicitly deal with bias introduced due to spot truncation, i.e. our wavefront reconstruction is slightly pessimistic, and could be improved upon in a separate study.

The LGS spots are truncated at the edge of the sub-apertures, and we assume that a field-stop is in place to prevent leakage between sub-apertures.
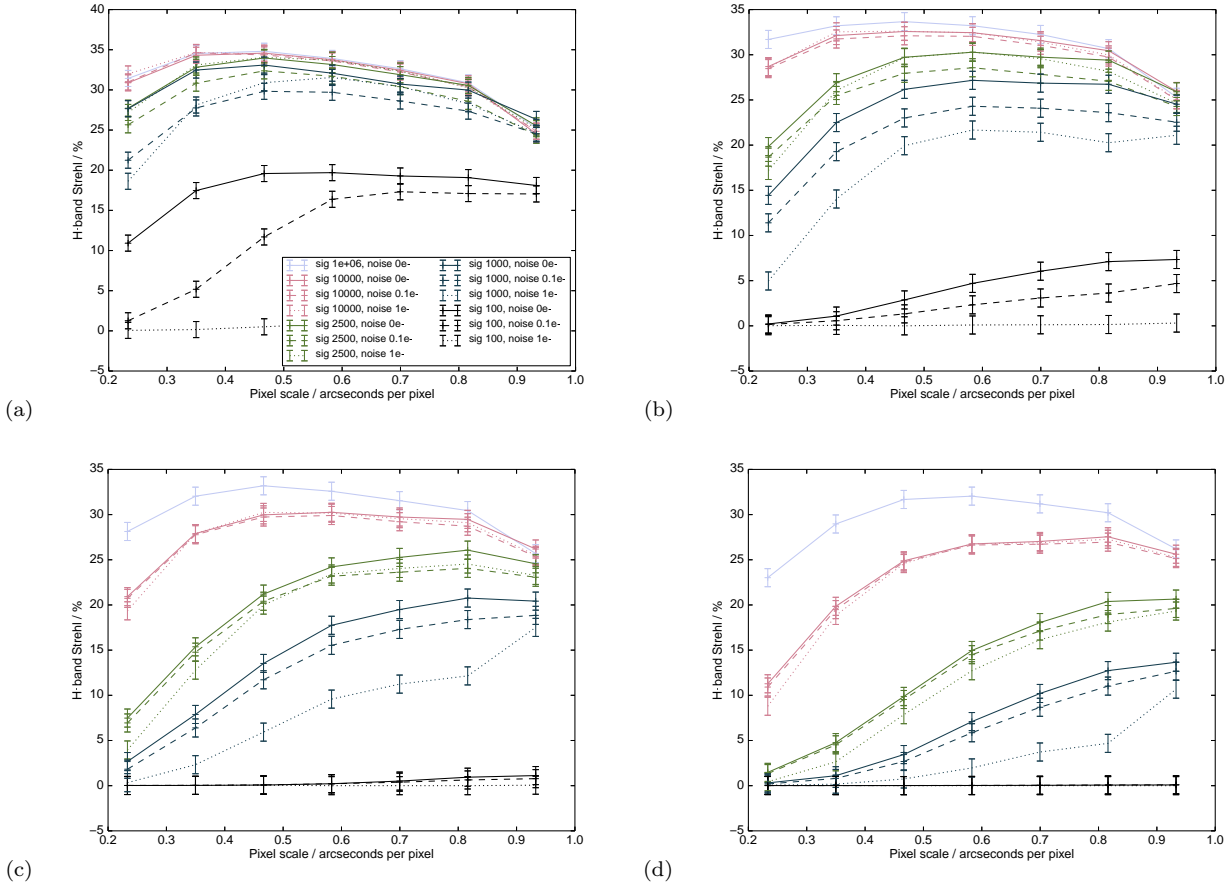
Figure 8. A figure showing on-axis AO performance (H-band Strehl) as a function of wavefront sensor pixel scale, for (a) a 5 km sodium layer FWHM, (b) a 10 km sodium layer FWHM, (c) a 15 km sodium layer FWHM and (d) a 20 km sodium layer FWHM. Different signal levels and readout noise levels are shown, as given by the legend in (a), using 16×16 pixel sub-apertures. In summary, from dark to light represents increasing photon flux (sig, in photons per sub-aperture per frame), solid lines have no readout noise, dashed lines have 0.1e- noise, and dotted lines have 1e- readout noise.

3.5 LGS sub-aperture size

Larger sub-apertures require detectors with more pixels, increased real-time control system (RTCS) computation power, more expensive detectors, and generally result in more costly AO systems. We therefore explore AO performance as a function of sub-aperture size (in terms of pixel count), in Fig. 10. It is evident here that larger sub-apertures are favourable, primarily to avoid spot truncation. With increased pixel scale (compressing the LGS PSF into fewer pixels), the number of pixels required (sub-aperture pixel size) can be reduced with little performance loss. However, with an increased sodium layer depth (more elongated spots), resulting in increased spot truncation for smaller sub-apertures, the pixel count cannot be reduced without a more significant effect on performance, and larger pixel count sub-apertures are favoured.

There is evidently a trade-off to be made, between sub-aperture size and system cost. We suggest that a minimum of 10×10 pixels per sub-aperture would be appropriate for a pixel scale of 0.7 arcseconds per pixel, with a total field of view of 7 arcseconds or more, though this is highly dependent on actual sodium layer profile. We note that this is a minimum requirement, and that greater performance

would be achieved using a larger number of pixels particularly when the sodium layer depth is more extensive, provided that readout noise does not dominate.

3.6 Operation with NGS

Fig. 11 shows predicted AO performance as a function of distance from the on-axis direction, for a system using 3 NGS for tip-tilt correction, and 6 LGS for higher order correction. This can be compared directly with Fig. 3(c), which uses only LGS (that are used unphysically for tip-tilt correction). Performance is very similar in both cases (though not identical), which confirms that the simplification made when using only LGSs is able to provide a reasonably reliable performance estimate. As stated previously, we note that actual performance will depend somewhat on NGS asterism shape and availability of suitably bright targets, though this is beyond the scope of the study presented here. In the case presented here, the 3 NGSs were in an asterism equally placed around a 2 arcminute diameter circle, as were the 6 LGS.
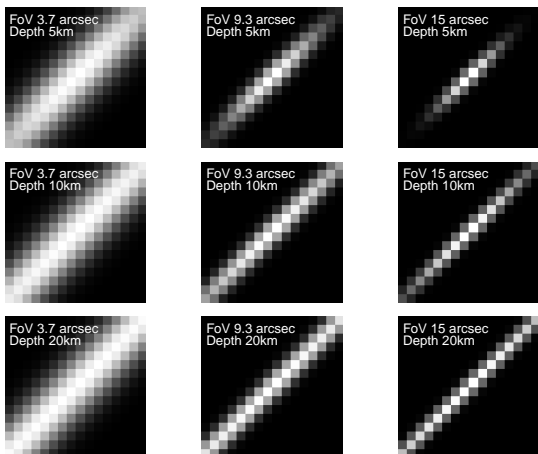
Figure 9. A figure showing a single sub-aperture as simulated here, 40 m from the laser launch location, for different sodium layer depths and pixel scales as given in the figure.
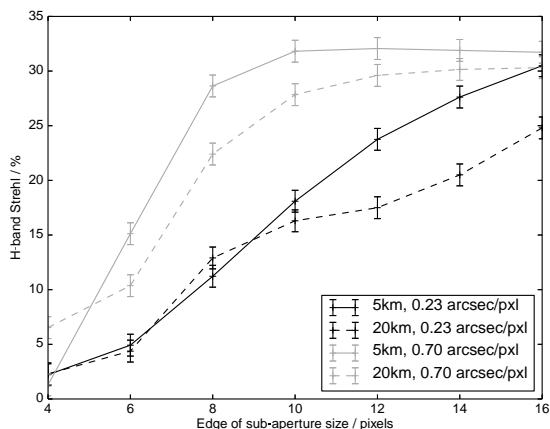

Figure 10. A figure showing on-axis AO performance as a function of sub-aperture size, for different pixel scales and sodium layer depths (as given in the legend).

3.7 Comparisons with other simulation results

A direct comparison with other previous simulation results is difficult, due to differences in atmospheric models, science wavelength, numbers of sub-apertures, telescope size and other modelling uncertainties and differences. However, verification of performance trends is possible. We find that our estimated performance for basic models is broadly similar to other ELT Monte-Carlo models (Le Louarn et al. 2012; Tallon et al. 2011; Foppiani et al. 2010), and slightly pessimistic when compared with analytical models of AO performance (Neichel et al. 2008), as expected. The consideration of DM conjugation is largely independent of telescope diameter, and our results are similar to those given by Femenía & Devaney (2003); Flicker et al. (2000). Similarly, a study of LGS pixel count was carried out by van Dam et al. (2011). A combined study of pixel scale, sodium layer depth and LGS signal level is new here.
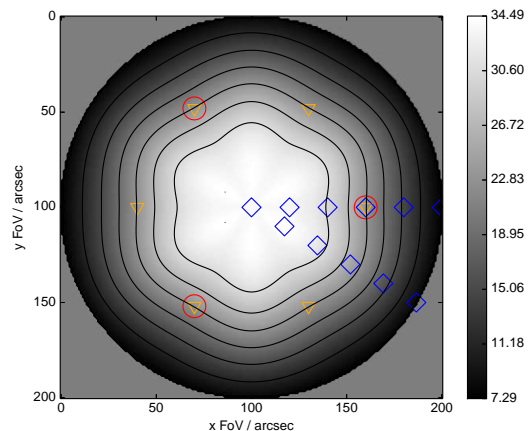

Figure 11. A figure showing Strehl across a 3.33 arcminute field of view for tip-tilt correction performed using 3 NGS, and higher order correction using 6 LGS. This can be compared directly with Fig. 3(c) which shows LGS correction only (i.e. tip-tilt correction is performed using the LGS). The LGS positions are shown by orange triangles, the NGS positions by red circles, and the science PSF sampling positions by blue diamonds.

4 CONCLUSIONS

We have performed AO performance modelling for a MCAO system on the E-ELT, using a Monte-Carlo, end-to-end AO simulation code, and have looked at number of LGSs, DM configuration, LGS pixel scale, and sodium layer depth. We find that using 6 LGS seems to be a good compromise between performance and cost. The use of 3 DMs, rather than 2 provides a significant performance advantage, though it is possible to reduce the actuator pitch of these DMs to below that of the WFSs, without significant performance loss, hence reducing system cost. We find that the ideal pixel scale and WFS field of view depends on sodium layer profile, and suggest that a field of view should be chosen that is sufficient to encompass all likely sodium layer profile depths. A pixel scale of at least 0.7 arcseconds per pixel is necessary, and at least 10×10 pixels per sub-aperture should be used, for the simplified Gaussian profiles used here. We note that this is likely to lead to spot truncation, and there is a trade-off between truncation and sensitivity. We also find that, as expected, larger sub-apertures (in terms of pixel count) offer better performance as this reduces clipping of the elongated LGS spots.

REFERENCES

Arcidiacono C., Schreiber L., Bregoli G., Diolaiti E., Foppiani I., Cosentino G., Lombini M., Butler R. C., Ciliegi

P., 2014, in Society of Photo-Optical Instrumentation Engineers (SPIE) Conference Series Vol. 9148 of Society of Photo-Optical Instrumentation Engineers (SPIE) Conference Series, End to end numerical simulations of the MAORY multiconjugate adaptive optics system. p. 6

Babcock H. W., 1953, Pub. Astron. Soc. Pacific, 65, 229

Basden A., 2015, JATIS, 1(3), 039002

Basden A. G., 2014, MNRAS, 440, 577

Basden A. G., Butterley T., Myers R. M., Wilson R. W., 2007, Appl. Optics, 46, 1089

Basden A. G., Evans C. J., Morris T. J., 2014, MNRAS, 445, 4008

Basden A. G., Myers R. M., 2012, MNRAS, 424, 1483

Bonaccini Calia D., , 2015, private communication, presentation at EWASS 2015

Clénet Y., Bernardi P., Chapron F., Gendron E., Rousset G., Hubert Z., Davies R., Thiel M., Tromp N., 2011, in Second International Conference on Adaptive Optics for Extremely Large Telescopes. Online at ¡A href="http://ao4elt2.lesia.obspm.fr"¿http://ao4elt2.lesia.obspm.fr¡/A¿, id.P23 The SCAO module of the E-ELT adaptive optics imaging camera MICADO. p. 23P

Ellerbroek B., Gilles L., Vogel C., 2003, Appl. Optics, 42, 4811

Femenía B., Devaney N., 2003, A&A, 404, 1165

Flicker R., Rigaut F. J., Ellerbroek B. L., 2000, in Wizinowich P. L., ed., Adaptive Optical Systems Technology Vol. 4007 of Society of Photo-Optical Instrumentation Engineers (SPIE) Conference Series, Comparison of multiconjugate adaptive optics configurations and control algorithms for the Gemini South 8-m telescope. pp 1032–1043

Foppiani I., Diolaiti E., Lombini M., Baruffolo A., Biliotti V., Bregoli G., Cosentino G., Delabre B., Marchetti E., Schreiber L., Conan J.-M., D'Odorico S., Hubin N., 2010, in Adaptative Optics for Extremely Large Telescopes MCAO for the E-ELT: preliminary design overview of the MAORY module. p. 2013

Foy R., Labeyrie A., 1985, A&A, 152, L29

Johns M., 2008, in Extremely Large Telescopes: Which Wavelengths? Retirement Symposium for Arne Ardeberg Vol. 6986, The giant magellan telescope (gmt). pp 698603–698603–12

Le Louarn M., Clare R., Bchet C., Tallon M., 2012 Vol. 8447, Simulations of adaptive optics systems for the e-elt. pp 84475D–84475D–7

Neichel B., Fusco T., Conan J.-M., 2008, Journal of the Optical Society of America A, 26, 219

Nelson J., Sanders G. H., 2008, in Society of Photo-Optical Instrumentation Engineers (SPIE) Conference Series Vol. 7012 of Society of Photo-Optical Instrumentation Engineers (SPIE) Conference Series, The status of the Thirty Meter Telescope project. pp 70121A–70121A–18

Otarola A., Neichel B., Wang L., Boyer C., Ellerbroek B., Rigaut F., 2013, in Esposito S., Fini L., eds, Proceedings of the Third AO4ELT Conference Analysis of fratricide effect observed with GeMS and its relevance for large aperture astronomical telescopes. p. 58

Rigaut F., Neichel B., Boccas M., d'Orgeville C., Arriagada G., Fesquet V., Diggs S. J., Marchant C., Gausach G., Rambold W. N., Luhrs J., Walker S., Carrasco-Damele

E. R., Edwards M. L., Pessev P., Galvez R. L., 2012, in Society of Photo-Optical Instrumentation Engineers (SPIE) Conference Series Vol. 8447 of Society of Photo-Optical Instrumentation Engineers (SPIE) Conference Series, GeMS: first on-sky results

Sarazin M., Le Louarn M., Ascenso J., Lombardi G., Navarrete J., 2013, in Adaptative Optics for Extremely Large Telescopes 3 Defining reference turbulence profiles for E-ELT AO performance simulations

Spyromilio J., Comerón F., D'Odorico S., Kissler-Patig M., Gilmozzi R., 2008, The Messenger, 133, 2

Tallon M., Béchet C., Tallon-Bosc I., Le Louarn M., Thiébaut É., Clare R., Marchetti E., 2011, in Second International Conference on Adaptive Optics for Extremely Large Telescopes. Online at ¡A href="http://ao4elt2.lesia.obspm.fr"¿http://ao4elt2.lesia.obspm.fr¡/A¿, id.63 Performance of MCAO on the E-ELT using the Fractal Iterative Method for fast atmospheric tomography. p. 63

van Dam M. A., Conan R., Bouchez A. H., Espeland B., 2011, in Second International Conference on Adaptive Optics for Extremely Large Telescopes. Online at ¡A href="http://ao4elt2.lesia.obspm.fr"¿http://ao4elt2.lesia.obspm.fr¡/A¿, id.67 Aberrations induced by side-projected laser guide stars in laser tomography adaptive optics systems. p. 67

This paper has been typeset from a TEX/ LATEX file prepared by the author.